# Characterization of Si-doped GaAs cross-sectional surfaces via *ab initio* simulations

Xiangmei Duan,[1,2] Maria Peressi,[1,3] and Stefano Baroni[1,4]
[1]*INFM-DEMOCRITOS National Simulation Center, Trieste, Italy*
[2]*Institute of Solid State Physics, Chinese Academy of Sciences, Hefei, People' Republic of China*
[3]*Dipartimento di Fisica Teorica, University of Trieste, Trieste, Italy*
[4]*Scuola Internazionale Superiore di Studi Avanzati, Trieste, Italy*
(Received 15 April 2005; revised manuscript received 25 June 2005; published 25 August 2005)

Si-doped (110) GaAs cross-sectional surfaces are investigated using first principles calculations with the aim of identifying simple configurations compatible with experimentally detected scanning tunneling microscopy (STM) images characterized by bright signals at negative bias and strongly attenuated when the bias is reversed. Since Si-donor is the most common defect in Si-doped GaAs, we study mainly several Si-donor based configurations, from the isolated impurity to extended defect configurations, up to the limit of an entire embedded donor interlayer. We consider also donor-acceptor configurations, stimulated by the experimental evidence of self-compensation effects in particular in highly doped samples. The systematic study of simulated cross-sectional STM images for all these and other configurations allows not only to identify the self-compensated donor-acceptor configurations as the simplest ones which are compatible with those experimental observations, but also to exclude most of the other candidates.

DOI: 10.1103/PhysRevB.72.085341 PACS number(s): 73.20.At, 73.20.Hb, 68.37.Ef

## I. INTRODUCTION

Defects play a key role on the properties of the semiconductors, and are often invoked to explain several effects, such as pinning of the Fermi level, variation in the surface chemical reactivity and in the diffusion at surfaces and interfaces. Si doped GaAs in particular has an outstanding technological importance for electronic devices. Remarkably, Si in GaAs has an amphoteric behavior, substituting both arsenic and gallium atoms as an acceptor or a donor, respectively.

It is rather difficult to obtain direct information about the local environment around the dopants or the defects in general. An approach which has been exploited in the last decade is to cut the material along a cleavage plane, so that the defects originally inside the crystal are exposed on a surface (a *cross-sectional surface*) and can be studied with the scanning tunneling microscopy (STM) and spectroscopy (STS),[1,2] surface-sensitive techniques with atomic-scale resolution which have been applied for a long time to *natural* surfaces.

The typical cleavage surface of polar zinc blende semiconductor is the (110) surface, which allows us to obtain usually large atomically flat surfaces and does not reconstruct. Therefore it is a very favorable geometry for the investigation of defects. Both clean and Si doped GaAs(110) surfaces are the subject of a vast literature, mainly experimental. Most of the results are summarized and reviewed in Ref. 2. More recent experimental studies are reported in Refs. 3–9: they include combined cross-sectional scanning tunneling microscopy (XSTM) and spectroscopy (XSTS) investigations of Si $\delta$-doped samples[3] and refined analysis of the clean surface obtained with promising improvements of the experimental technique, which—making use of semiconductor tips—enables state-specific energy-filtered imaging.[9]

A few theoretical studies of Si-doped or otherwise defected GaAs surface exist,[10–15] and the concerted experimental and theoretical efforts have been able to clarify the microscopic picture of several common defects. Nonetheless, not all the defects visible in the experimental images have been clearly hitherto identified. Only recently we have shown that donor-acceptor configurations give XSTM images which are consistent with the experimental ones of self-compensated Si-doped samples, characterized by strong bright signals at negative bias and strongly attenuated when the bias is reversed.[16] We complete here this investigation, by exploiting whether these fingerprints can be found in other simple defected configurations. The study mainly concerns donor and donor-acceptor configurations, as suggested by the experimental evidence of the Si-donor as the most common defect in Si-doped samples and by the existence of self-compensation effects in highly doped samples. For the sake of comparison, we investigate also a few other selected configurations with isolated vacancies or antisites, or donor-vacancy complexes.

Some technical details of the calculations are explained in the next section. In Sec. III we report the main results for the cases studied, in terms of structural and electronic properties of the exposed surface, including XSTM simulated images at different bias voltages and atomic-projected local density of states. In Sec. IV we draw our conclusions. Appendices A and B report for comparison also some results for defects other than Si donors and donor-acceptors.

## II. THE THEORETICAL APPROACH

The study of cross-sectional surfaces is conceptually similar to that of natural surfaces, although it is affected by additional technical difficulties due to the unconventional surface geometry which requires the use of large simulation cells to model the systems. We use supercells with a (110) slab geometry. Periodic boundary conditions are applied along all the $(1\bar{1}0)$, (110), and (001) directions. In the former

 

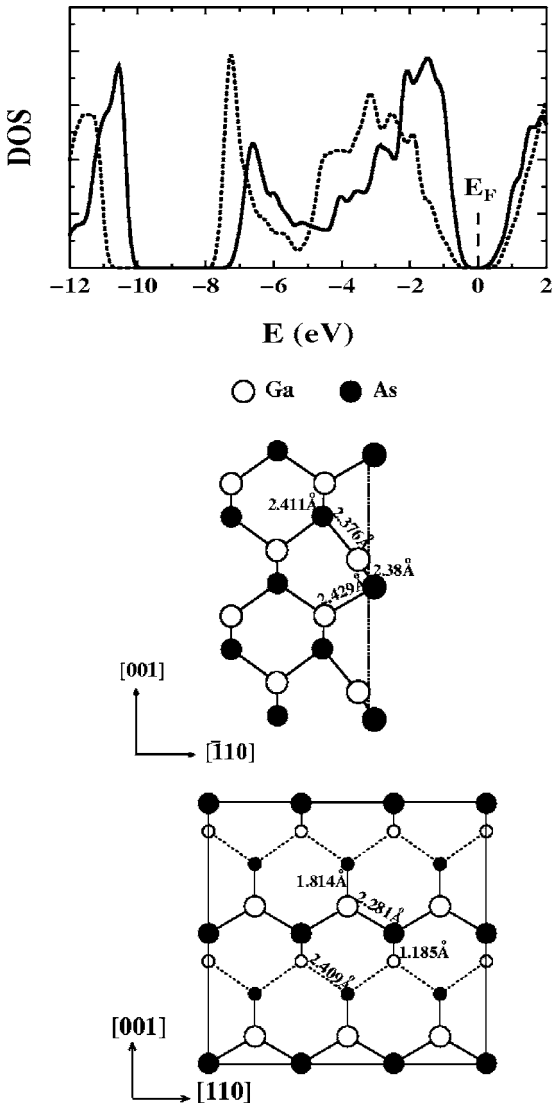


FIG. 1. Clean (110) GaAs surface. Top and middle panels: ball and stick model of the relaxed surface, side (top panel), and top view (middle panel). The unrelaxed surface position is indicated by a solid line in the topmost panel. In the side view we indicate the bond lengths values; in the top view we indicate the surface-projected values of the bond lengths. Bottom panel: density of states (arbitrary units) of the surface atoms (solid line) and of bulk GaAs (dotted line).

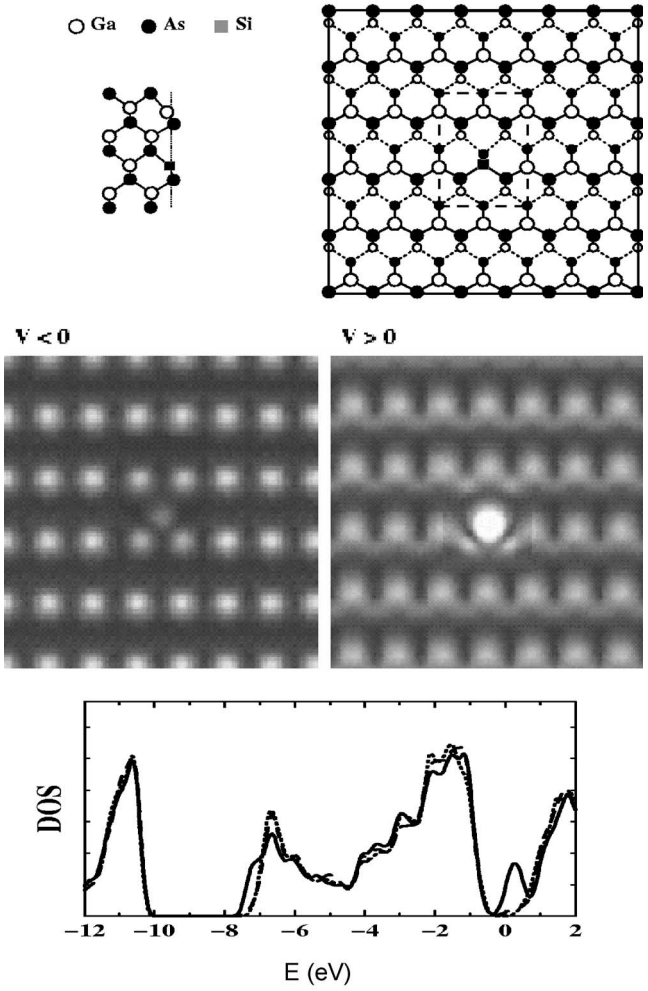


FIG. 2. A neutral single substitutional surface $Si_{Ga}$ impurity. Top panels: see Fig. 1 for caption. The long-dashed lines in the top-view ball and stick model indicate the cell used to simulate the XSTM image of the defected region, which is superimposed to the image of the otherwise perfect clean surface for a better visual rendering. Middle panels: corresponding simulated XSTM images at bias voltages of −1 eV (left) and +1 eV (right). Bottom panels: density of states of surface atoms belonging to the simulation cell with the defect (solid line); Ga and As surface atoms far from the defect but belonging to the simulation cell, for alignment with the density of states of the clean surface (dashed line); clean surface, from Fig. 1, for comparison (dotted line). The midgap peak in the DOS of the doped cell is originated by the impurity.

direction they are used to describe repeated parallel slabs (containing 9 atomic planes), separated by a vacuum region (of about 12 Å in our case) large enough to guarantee a sufficient separation of two adjacent surfaces. The periodic boundary conditions along the (110) and (001) directions are used instead to describe the infinite surface. The unit cell of the clean surface contains only 2 surface atoms, but this number rapidly increases for doped configurations, depending on their complexity: it contains up to 20 surface atoms in our cases. The supercell size in each direction has to be large enough in order to guarantee a sufficient separation between periodic images of the defects.

Our numerical approach is based on the plane-wave pseudopotential method in the framework of density functional theory (DFT) within the local-density approximation (LDA), using the ESPRESSO/PWscf code.[17] We use pseudopotentials with the Perdew-Zunger exchange-correlation functional. The plane wave basis set is expanded up to a kinetic energy cutoff of 14 Ry. The Brillouin-zone integration is performed using the Gaussian-broadening special-point technique: for the unit cell (clean surface) we use a $6\times4\times1$ mesh for self-consistent calculations and a $12\times8\times2$ mesh for nonself-consistent calculations of densities of states and STM images; similar meshes, properly folded, are chosen for the geometries of the doped configurations. The smearing parameter is equal to 0.01 Ry.

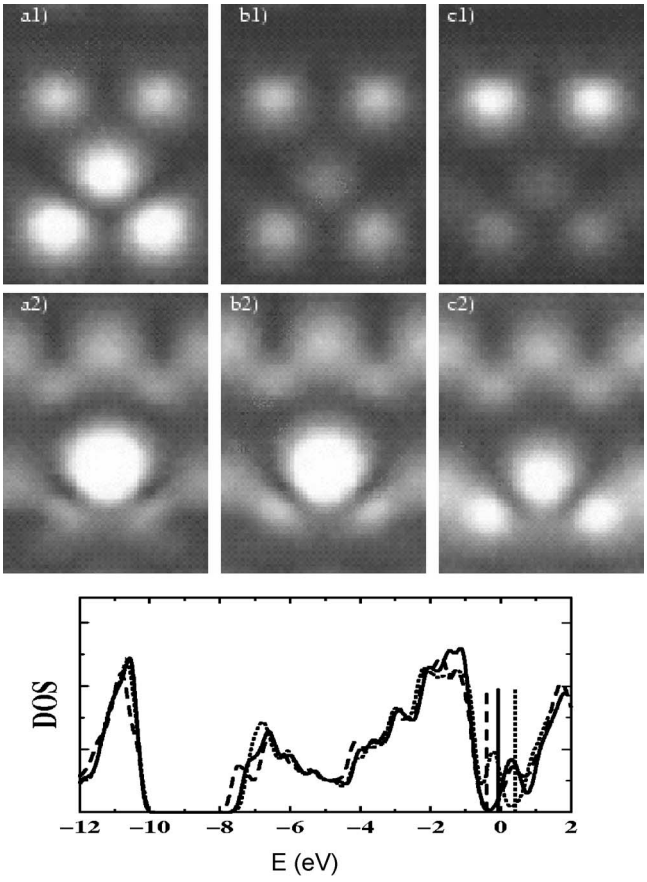


FIG. 3. A single substitutional surface $Si_{Ga}$ impurity with different charge states. Top panels: STM images at bias voltages of +1 eV [a1), b1), c1) panels] and −1 eV [a2), b2), c2) panels] for negatively (−1 electron per defect; left panels), neutral (central panels), and positively charged samples (−1 electron per defect; right panels). Bottom panel: corresponding surface density of states aligned with respect to the band gap edges of the clean surface: negatively (long-dashed), neutral (solid), and positively (dotted) charged cases. Corresponding calculated Fermi energies are also indicated.

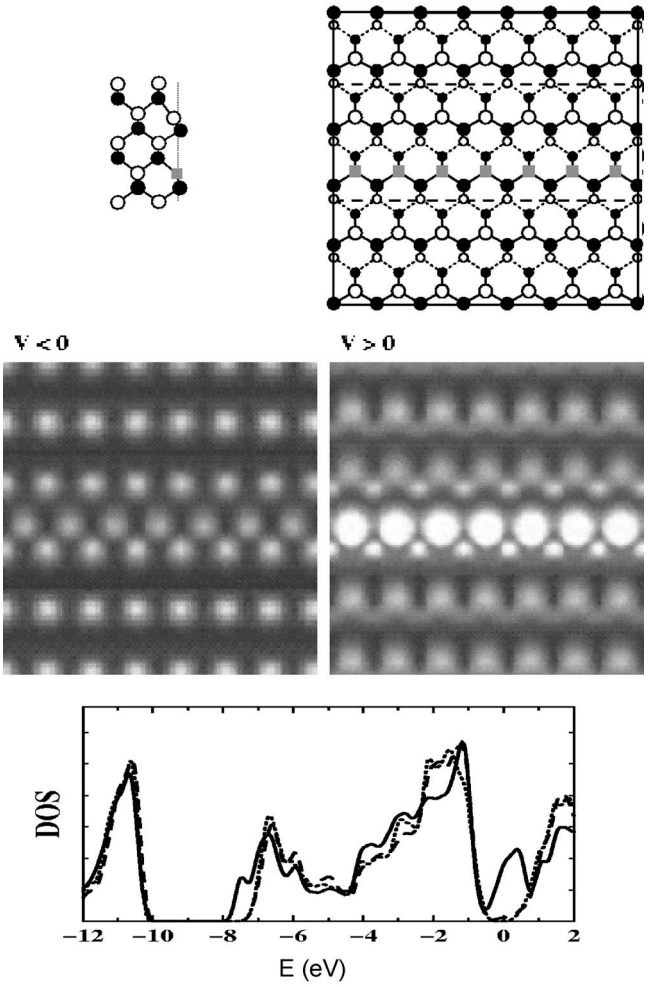


FIG. 4. A row of $Si_{Ga}$ donors on the surface. For this figure and the following ones, see Fig. 2 for caption, if not differently indicated.

The calculated equilibrium lattice parameter for bulk GaAs is 5.56 Å, which compares well with the experimental datum (5.55 Å); similar agreement is found also for other structural parameters such as the elastic constants, thus allowing us to study lattice relaxations on a realistic ground. The calculated energy gap for bulk GaAs is 1.36 eV, slightly underestimated with respect to the experimental value of 1.52 eV, as it typically occurs in DFT-LDA calculations.

STM images are obtained with the simple model by Tersoff and Hamann (TH).[18] According to this model, the tunneling current is approximately given by

$$I(V) \propto \int_{E_F}^{E_F+eV_b} \rho(\mathbf{r},\epsilon)d\epsilon, \tag{1}$$

where $\rho(\mathbf{r},\epsilon)$ is the local density of states (LDOS) at the position $\mathbf{r}$ of the tip and energy $\epsilon$, $E_F$ is the Fermi energy, and $V_b$ the applied bias. The TH model is essentially a first-order perturbation theory, which does not take into account tip-surface interaction and hence in general it can be applied at fairly large tip-surface separation. In this model the proximity of the tip is assumed not to perturb the electronic structure of the surface. Despite its simplicity and the severe approximations used, the model has been widely applied to metals and semiconductors surfaces, and it is able to provide, at least qualitatively, a correct description of STM images. Extensions of this model allow to consider also the possibility of $p$ or $d$ character orbitals of the tip.[19,20] Alternative approaches aimed at treating the system and the tip together have been proposed, for instance make use of the semiempirical extended Huckel theory for a treatment of the tip-sample interaction,[21] or combining DFT approach with the Kubo-Greenwood formalism for the conductivity,[22] or using the TH approach but modeling also the tip in terms of ions and electrons and treating the tip-surface system as a whole.[23,24]

The position of the calculated Fermi energy depends sensitively on the concentration of the dopants which is contrivedly large, for it depends on the size of the supercell. To cope with this difficulty we align the surface LDOS of the doped samples far from any impurities with the corresponding LDOS of the clean surface, and then we refer the simulated

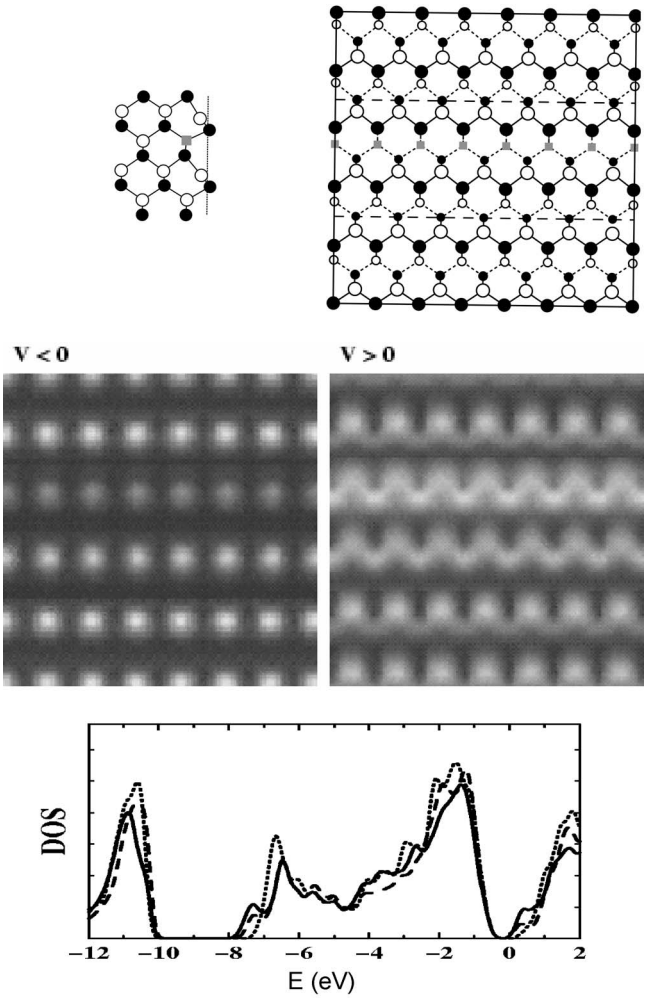


FIG. 5. A row of $Si_{Ga}$ donors subsurface.

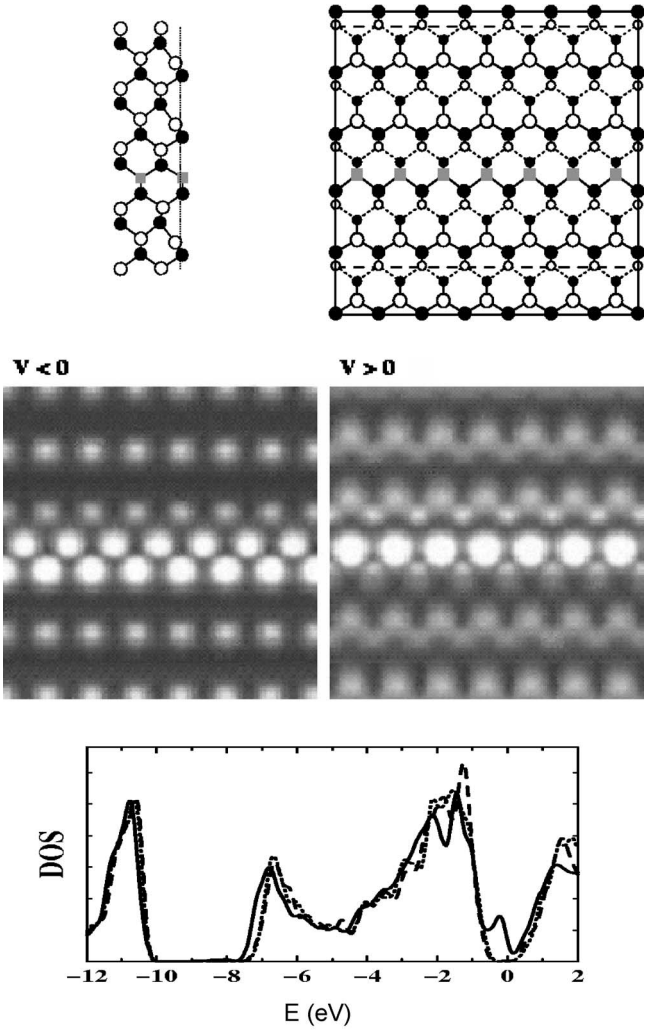


FIG. 6. 1 ML of $Si_{Ga}$ embedded in GaAs along the (001) direction, with the (110) cleavage plane containing $Si_{Ga}$ and As sites (case A in the text).

XSTM images to the Fermi energy in the midgap position, corresponding to the case of the neutral undoped surface at 0 K. In the experimental samples the Fermi energy depends on the overall doping and can be more close to the conduction or valence band edges, for *n*- or *p*-doping, respectively. We account for that, in particular when we consider the case of a full bilayer of Si embedded in GaAs, whose experimental samples that we refer to are *n*-doped.

We mainly study neutral configurations. However, diffused as well as localized doping and the presence of the surface may affect the electronic structure of the sample not only by rigidly shifting band structure and LDOS with respect to the Fermi energy but also by modifying their shape. In order to estimate these effects we also examine some charge states of the samples and we investigate the changes in the structural and electronic properties in a self-consistent way. Charged systems require special care when treated with periodic supercells: we deal with them by adding a neutralizing uniform background.

## III. THE STRUCTURES CONSIDERED

With the aim of identifying the most important fingerprints of different defected configurations, we systematically examine several simple configurations with different kinds, concentrations and positions of defects. We start from configurations with Si donors only, since $Si_{Ga}$ is the most common defect in Si-doped GaAs samples: from the isolated $Si_{Ga}$ up to an entire row and an entire layer. We study then configurations based on donor-acceptor pairs, $Si_{Ga}$-$Si_{As}$, which are likely to occur in samples with high concentration of Si dopants, above the onset of self-compensation. Also in this case, we extensively study the possibility of different concentrations and configurations, from the isolated pair on-surface or subsurface, up to an entire Si (001) bilayer embedded in GaAs and exposed by cleavage to the (110) surface.

For completeness, we extend the investigation to other kinds of defects, and we report in the Appendix the details: configurations where Si donors are accompanied by vacancies, namely, $Si_{Ga}$-$V_{Ga}$ and $Si_{Ga}$-$V_{As}$ complexes (Appendix A) and other isolated defects not involving Si, i.e., surface or subsurface vacancies and antisites (Appendix B).

For each configuration we study the equilibrium geometry and the electronic structure, namely energy resolved surface

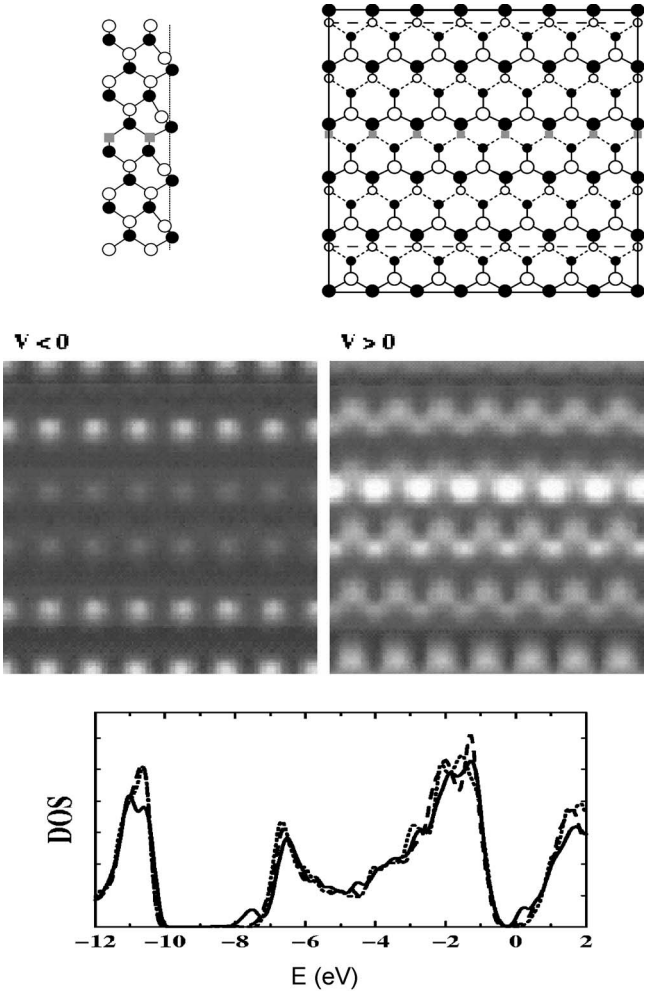


FIG. 7. 1 ML of $Si_{Ga}$ embedded in GaAs along the (001) direction, with the (110) cleavage plane containing unperturbed Ga and As sites only (case B in the text).

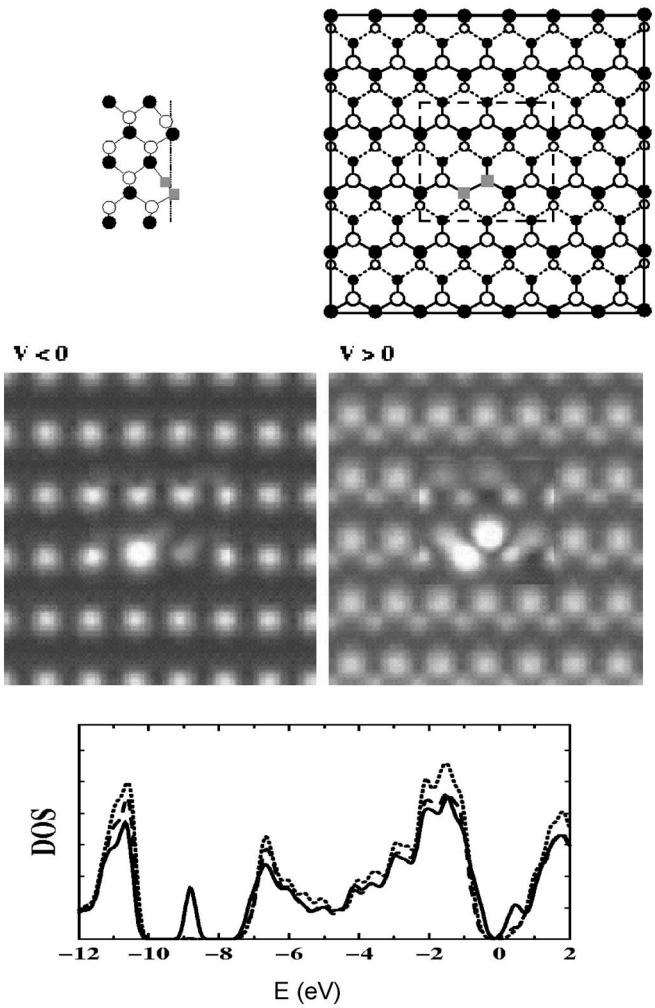


FIG. 8. $Si_{As}$-$Si_{Ga}$ dimer on the surface (dimer A in the text).

density of states and STM images. We stress that it is important to simulate STM images at different bias voltages in order to shed light on the identification of defects. In fact, it may occur that two defected configurations are not distinguishable on the basis of a unique STM image taken at one particular bias voltage. For each configuration studied we show a figure containing: from top to bottom and from left to right, side and front views of the relaxed underlying structure; STM images at negative and positive bias voltages ($V=-1.0$ eV and +1.0 eV, if other values are not specified), and surface DOS for: defected surface, all atoms (solid line); clean surface (dotted line, for comparison); defected surface, projected only onto Ga and As atoms far from the defect (dashed line, for the alignment of the DOS). The size of the entire region shown in our simulated STM images corresponds to $a \approx 3$ nm $\times 3$ nm.

### A. Clean GaAs(110) surface

We start considering the clean (110) surface. It does not reconstruct, but it shows some buckling due to the outward/inward relaxation of the As/Ga atoms (Fig. 1, upper panel). The buckling structure is characterized by an angle of 30.6°, and by a difference of 0.68 Å between the height of the surface As and Ga atoms, whose relative distance (2.38 Å) is almost unchanged with respect to the ideal bulk bond length (2.41 Å). Because of the buckling, the top-view projected geometry of the surface shows rows of (001)-oriented Ga-As pairs (visible with transmission electron microscopy, for instance) which are "long" (1.81 Å) if Ga is on surface and As subsurface and "short" (1.18 Å) in the complementary case.

The clean surface is semiconducting as in other III-V binary compounds.[25] The calculated energy gap is smaller than the bulk value by about 0.5 eV (see bottom panel of Fig. 1); this is mainly due to the topmost occupied surface As-$p$ states which are pushed at higher energies, because surface As atoms are in a potential less attractive than in the bulk crystal. The energy position of surface states is however at the edge or outside the band gap and does not obscure the defects we are interested in. Beside the easy cleavage and the unreconstructed geometry, this is an additional important feature of the (110) cross-sectional surfaces.

With STM, As atoms are visible at negative bias since they contribute to the valence band edge, while Ga atoms are seen at positive bias corresponding to empty states at the

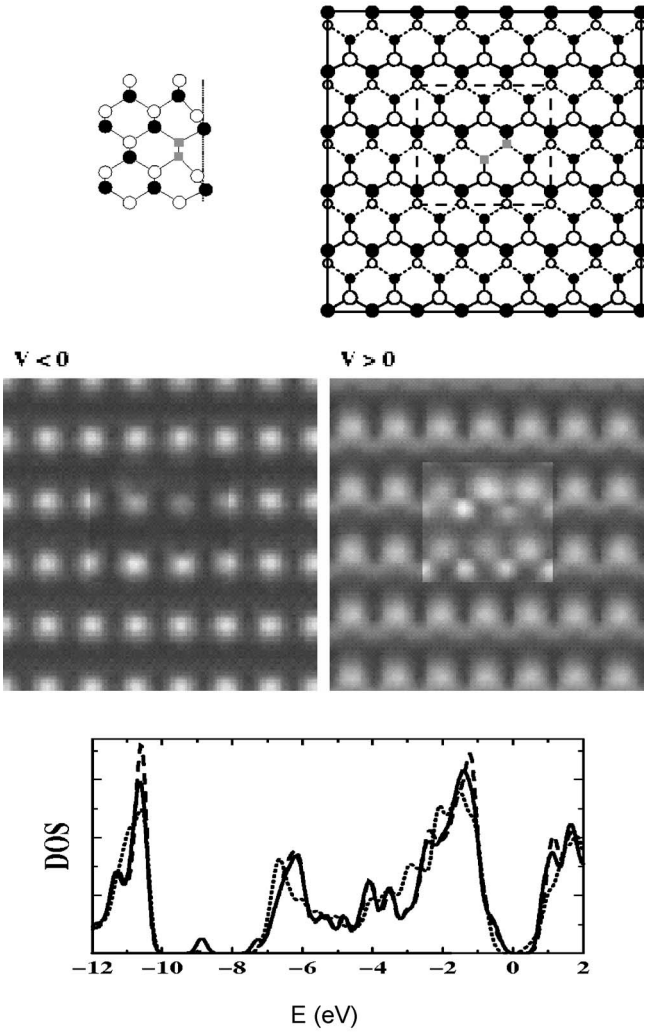


FIG. 9. $Si_{As}$-$Si_{Ga}$ dimer with $Si_{Ga}$ and $Si_{As}$ both subsurface (dimer B in the text).

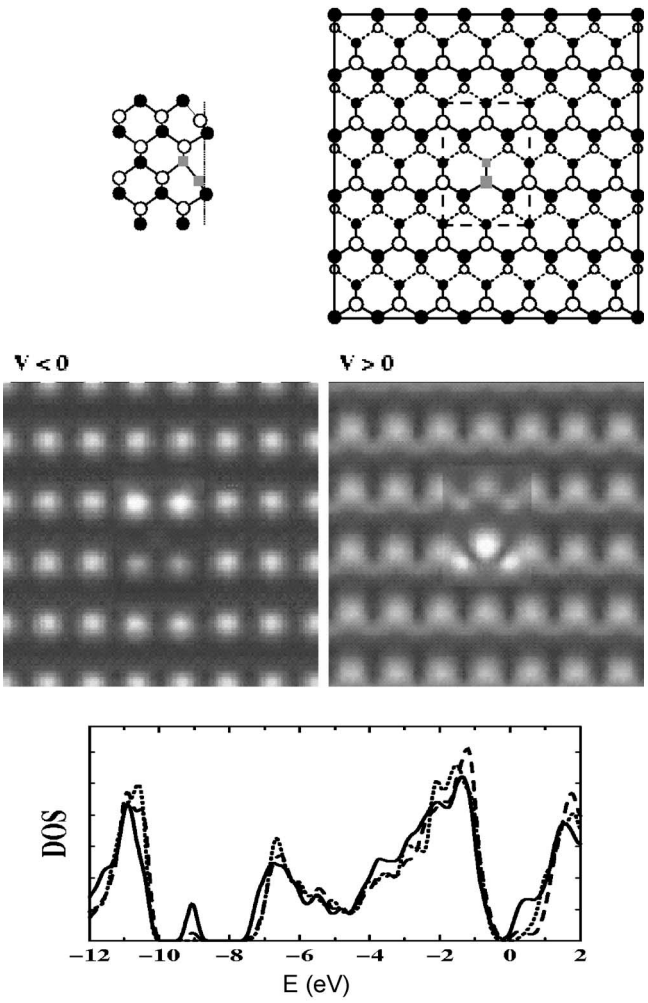


FIG. 10. $Si_{As}$-$Si_{Ga}$ dimer with only $Si_{Ga}$ on the surface and $Si_{As}$ subsurface (dimer C in the text).

bottom of the conduction band. The image of the clean surface can be seen in all the figures that we show for the defected configurations, looking at regions far from the defects. Our results confirm the findings of previous experimental and theoretical investigations,[10,26–28] thus validating our approach.

### B. Substitutional defects with $Si_{Ga}$ only

#### *1. Isolated* $Si_{Ga}$ *on the surface*

Our results for the isolated $Si_{Ga}$ on surface are shown in Fig. 2. For this case several experimental data, already fully interpreted, and previous numerical simulations are available for comparison. We repeat such calculations also as a benchmark for comparison with the other new defected structures here considered. The Si atoms tend to recover the position of an ideal truncated zinc blende structure, thus reducing the buckling from 0.68 Å to 0.37 Å. In the STM images we can easily recognize the fingerprint of $Si_{Ga}$ donor with a bright almost spherical spot mainly at positive bias (empty states). The two surface As atoms nearest neighbors (NN) to $Si_{Ga}$ are also visible with two smaller and less bright structures close to the large spot of the impurity. The $Si_{Ga}$ donor is also visible at negative bias, with a structure which appears as interstitial with respect to the regular grid formed by the occupied surface As states. The bright spot is due to a very localized density of states in the midgap, as shown in the bottom panel of Fig. 2.

Our calculations compare well with the observed STM images[2,3,29,30] and with previous calculated plots[10] at positive bias. The agreement with previous results at negative bias is less satisfactory. When making such comparison, however, we have to consider the sensitivity of the STM images to several factors, such as tunneling voltage (see, for instance, Fig. 4 of Ref. 30 or Fig. 2 of Ref. 31), nature and shape of the tip in case of experimental images, and specific theoretical approach and details such as choice of pseudopotentials, $k$ point sets for Brillouin zone samplings, size of the cell, in case of simulated images.

For the isolated $Si_{Ga}$ on surface we also show the results for positive and negative charge states (Fig. 3). The projected DOS for the positive charge state is similar in shape to the neutral state, with a peak close to the bottom of the conduction band when aligning the band edges with respect to the

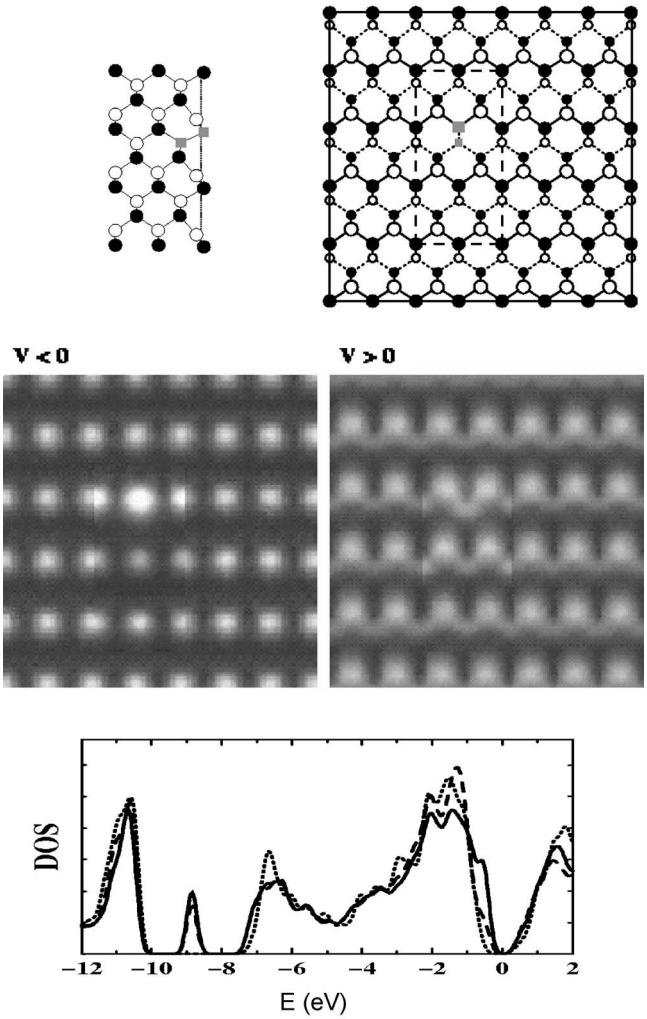


FIG. 11. $Si_{As}$-$Si_{Ga}$ dimer with only $Si_{As}$ on the surface and $Si_{Ga}$ subsurface (dimer D in the text).

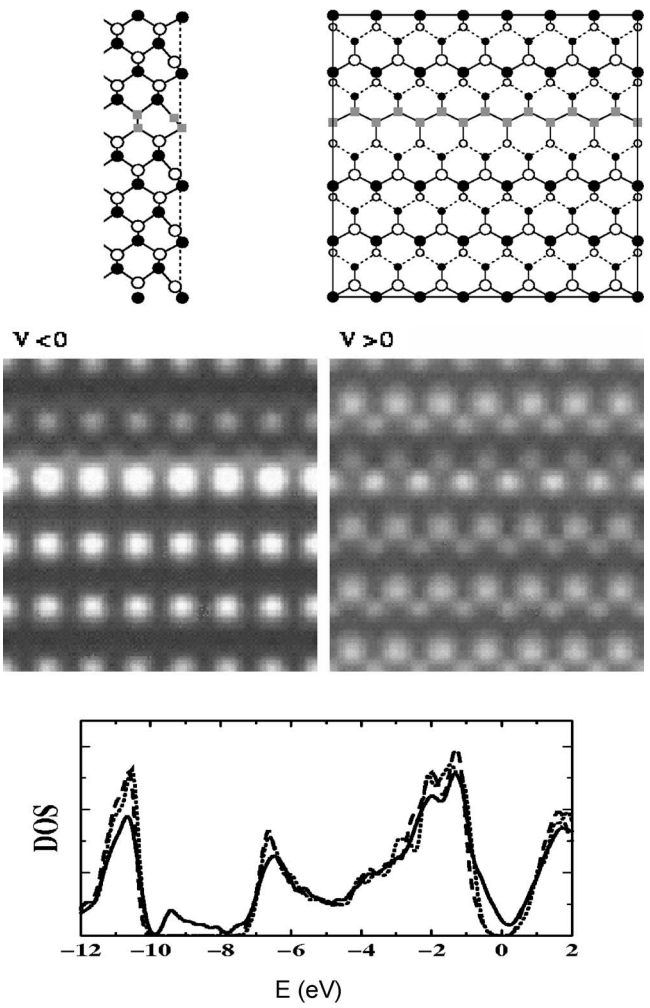


FIG. 12. Si bilayer with $Si_{As}$ and $Si_{Ga}$ on the surface (case A in the text).

case of the clean surface. In case of negative charge state, the induced impurity states are close to valence band maximum, thus resulting in a STM image of the occupied states showing more bright $Si_{Ga}$ and neighboring As also at negative bias. In Fig. 3 we have also indicated the Fermi energy as obtained from our supercell calculations; this has to be considered as qualitative only, as previously stressed, due to its strong dependence on the concentration of defects. We conclude that in this case the charge state can have noticeable influence on the STM images.

#### *2. Clusters of* $Si_{Ga}$ *on the surface*

We want to examine now the effect of progressively increasing the surface donor concentration; although the detailed shape of the DOS depends on the relative positions of dopants, in general the main feature for clusters of Si donors remains a peak induced in the gap, like for the isolated donor but with a larger broadening due to the increased interaction between the impurities. Two surface donors can be next nearest neighbors when they are close together in the (110) direction: even in such a case, the resulting STM images (not shown here) are in practice the superposition of the images of two isolated $Si_{Ga}$, with the surface As atom in between which appears more bright at negative bias voltage.

The interaction between the impurities is further enhanced in the case of an entire row of surface $Si_{Ga}$ (Fig. 4). It appears as a very bright line at positive bias, corresponding to a huge midgap peak in the surface DOS. The line is broadened over two atomic rows in case of negative bias, including the occupied states of surface $Si_{Ga}$ and their nearest neighbor surface As.

#### *3.* $Si_{Ga}$ *subsurface*

If donors are subsurface, we find in general that their STM images at negative bias are much less bright if compared with surface donors, both in the case of isolated $Si_{Ga}$ and of a row of $Si_{Ga}$. This is consistent with many experimental observations for the isolated $Si_{Ga}$ subsurface, including the early work of Zheng,[32] that report more delocalized and less pronounced features. Some experimental images instead seem to indicate more bright features compared with our calculations.[30] We show here our calculated STM images for a row of subsurface donors (Fig. 5). It is characterized by

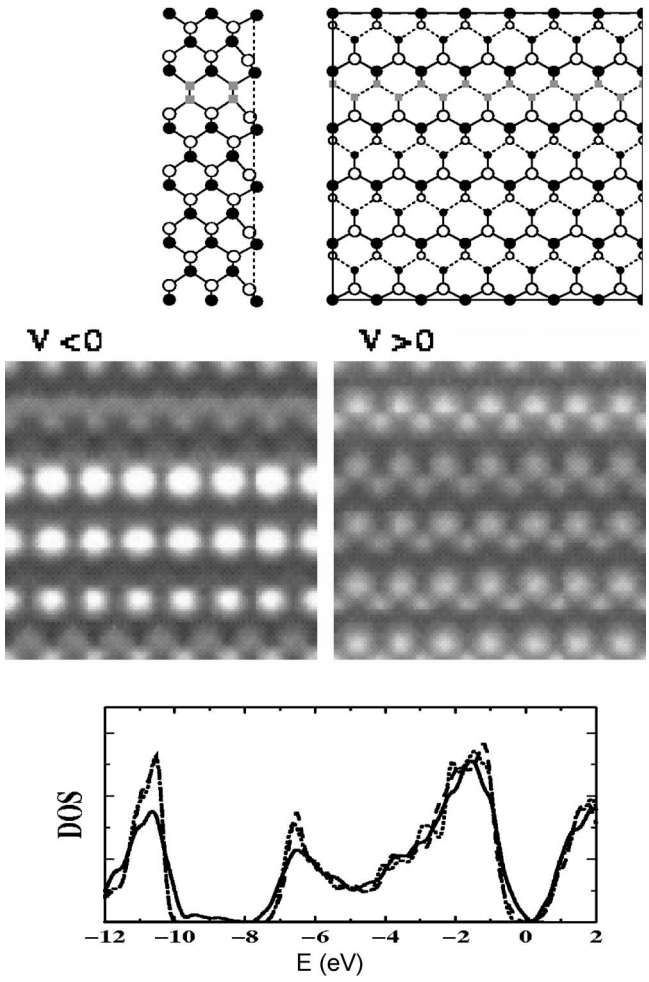


FIG. 13. Si bilayer with $Si_{Ga}$ and $Si_{As}$ both subsurface (case B in the text).

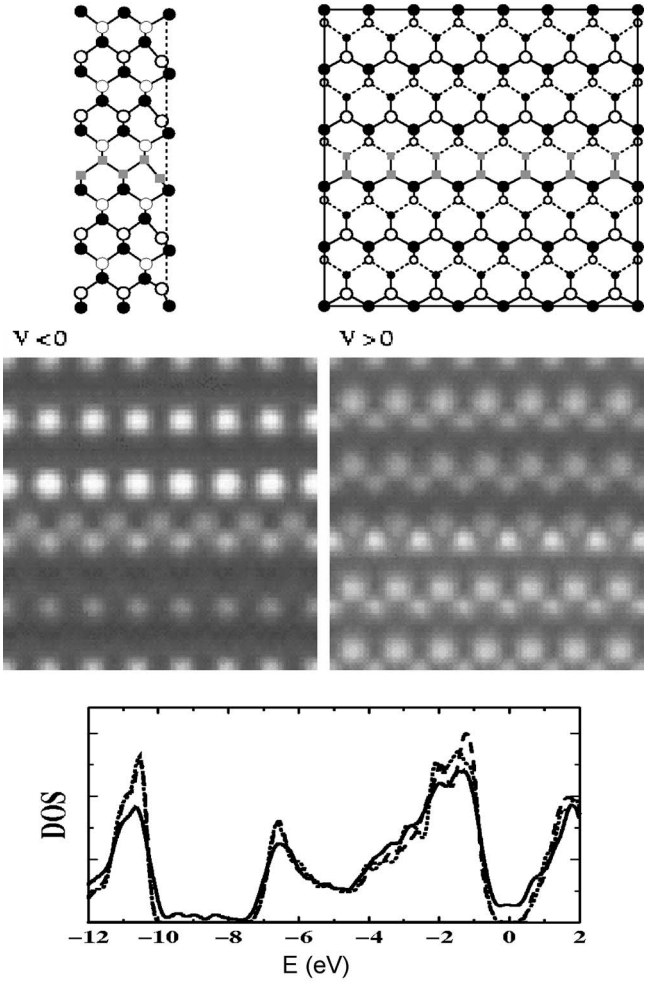


FIG. 14. Si bilayer with only $Si_{Ga}$ on the surface and $Si_{As}$ subsurface (case C in the text).

smoother features if compared with the on-surface case (Fig. 4). In particular, there is no evidence of Si empty states at negative bias, but rather the region surrounding the row of impurities is globally darker. An interesting feature of the presence of $Si_{Ga}$ subsurface is to enhance the surface buckling (left topmost panel of Fig. 5), since the Ga surface atoms near the defect tend to relax further inward with respect to the clean surface. This can contribute to the reduction of the signal of the subsurface $Si_{Ga}$, since the STM images are always the combined result of electronic and topographic effects.

#### *4. 1 ML of* $Si_{Ga}$

Considering the possible scenarios arising from a progressively higher Si doping of GaAs we come now to the case of an entire (001) ML of $Si_{Ga}$, shown in Figs. 6 and 7. The cleavage plane can contain the $Si_{Ga}$ and As sites (A, Fig. 6) or, alternatively, Ga and As sites only (B, Fig. 7). The geometry projected onto the surface is therefore similar to the case of a row of $Si_{Ga}$ on surface or subsurface, and also gives similar STM images. Figure 6 therefore compares well with Fig. 4, but it shows a more pronounced brightness at negative bias, corresponding to a peak in the gap closer to the valence band edge. Similarly, the case where the cleavage surface does not contain the impurity atoms (Fig. 7) can be compared with the case of 1 row of $Si_{Ga}$ subsurface (Fig. 5), showing similar features, although with different intensity.

We have also considered Si donors distributed over two adjacent cationic planes. In such a case (not shown here) a bright line still appears both at positive and negative bias—as in the case of 1 entire ML of $Si_{Ga}$—but with reduced intensity.

### C. Donor-acceptor configurations

By exploiting the amphoteric behavior of Si in GaAs, we study now configurations based on donor-acceptor $Si_{As}$-$Si_{Ga}$ pairs, from the isolated case to an entire bilayer embedded in the (001) direction. Such configurations are self-compensating and are likely to occur in particular in heavily Si doped samples. Considering a pair of impurities or a bilayer, different configurations are possible according to the specific position of the impurities with respect to the exposed surface: donors/acceptors can be in surface/subsurface positions, just considering only the first two layers.

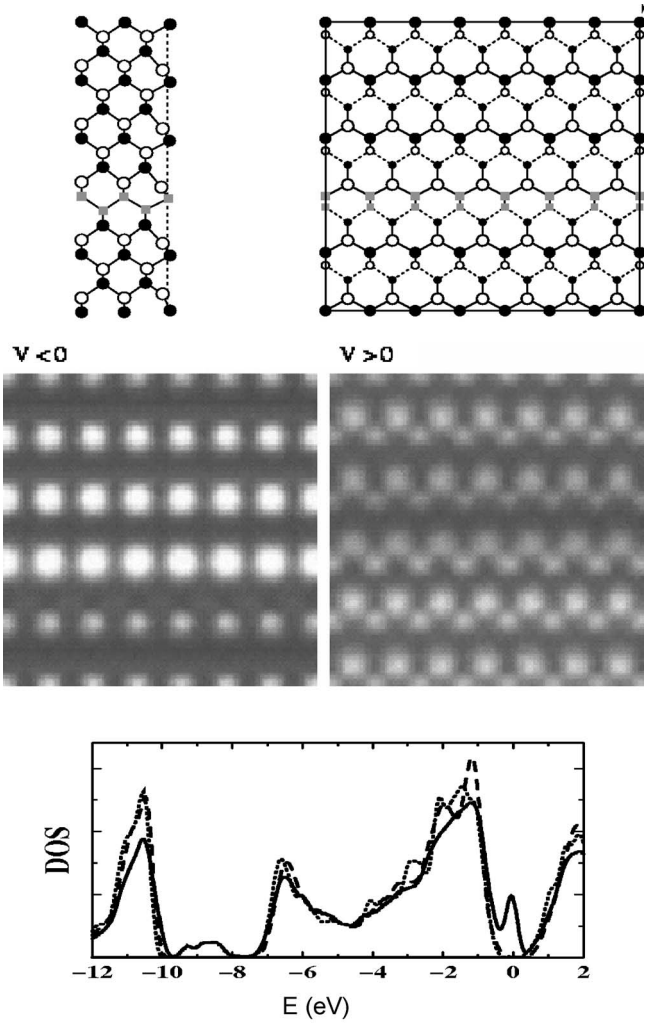


FIG. 15. Si bilayer with only $Si_{As}$ on the surface and $Si_{Ga}$ subsurface (case D in the text).

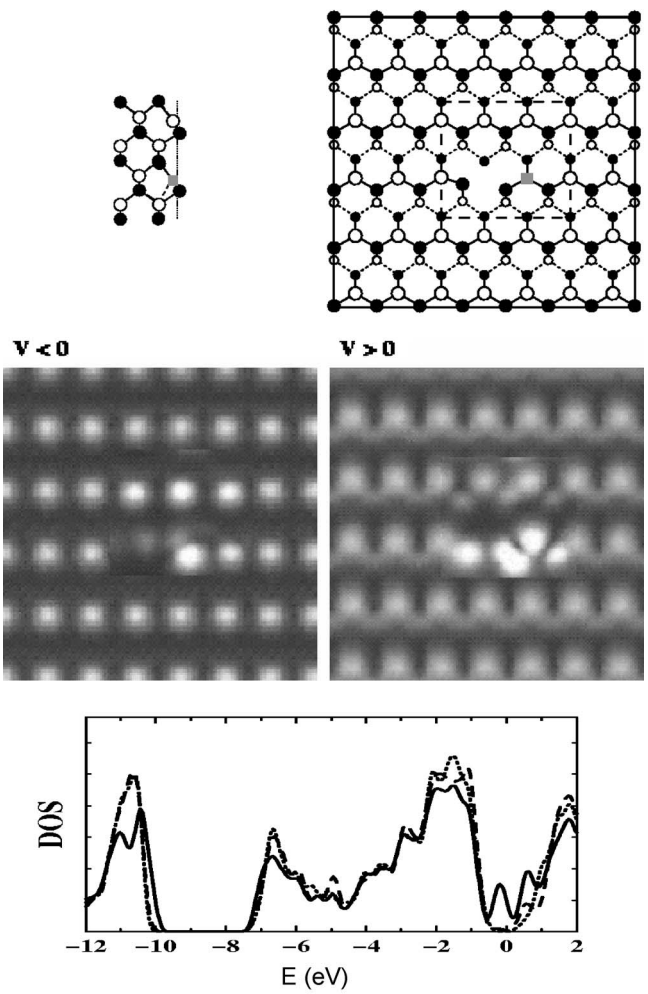


FIG. 16. Donor-vacancy complex: both $Si_{Ga}$ and $V_{Ga}$ on the surface.

#### *1.* $Si_{Ga}$-$Si_{As}$ *isolated pairs*

We consider the four different possible configurations for the isolated dimers: both $Si_{Ga}$ and $Si_{As}$ on surface (for simplicity we indicate it as case A in the following discussion); both subsurface (case B); only $Si_{Ga}$ on surface and $Si_{As}$ subsurface (case C); $Si_{As}$ on surface and $Si_{Ga}$ subsurface (case D). The results are shown in Figs. 8–11, respectively.

For dimer A, the $Si_{As}$ atom induces a bright spot at negative bias voltage, while at positive voltage both Si atoms contribute to the density of state. $Si_{Ga}$ atom shows a bright spot like in isolated $Si_{Ga}$ case. Dimer B does not show any particularly relevant feature. For dimer C, the main feature of STM images is a depression of occupied states around the defect and an increase of empty states as shown in Fig. 9. At positive voltage, the STM image is again similar to that of the isolated $Si_{Ga}$ impurity, except for the two surface As atoms neighbor to $Si_{Ga}$ which are brighter in this case. In case D the $Si_{As}$ atom and the two NNN As atoms in the same bond chain appear as brighter spots at negative voltage, whereas the signal is strongly attenuated at positive bias voltages. In all cases, the LDOS shows an additional peak in the ionicity gap which is characteristic of the $Si_{As}$ substitution.

#### *2.* $Si_{Ga}$-$Si_{As}$ *(001) bilayers*

When Si substitutes both Ga and As atoms in consecutive GaAs (001) atomic layers, the resulting configuration is a (001) Si bilayer embedded in GaAs and corresponding to a *microscopic capacitor* with unique electronic properties.[36,37] A self-compensating layer configuration is required by electrostatic stability, whereas its confinement and the value of the resulting dipole are limited by atomic interdiffusion. We study here the simplest possible configurations, i.e., an entire Si (001) bilayer confined onto two adjacent atomic planes and the case of one monolayer uniformly distributed over two such planes.

The intersection of the (110) surface with the Si (001) bilayer can occur in different positions and thus result in different configurations of the exposed surface that can include rows of Si atoms in As and/or Ga sites. Similarly to the isolated dimers, there are four different possible configurations: (A) both $Si_{Ga}$ and $Si_{As}$ on surface, forming a zig-zag

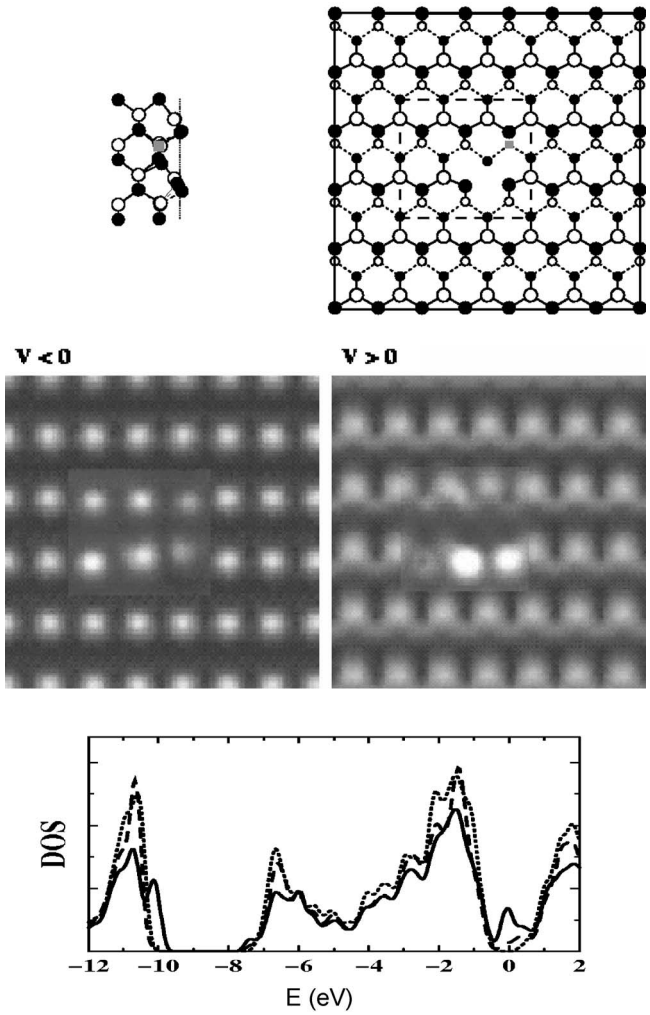


FIG. 17. Donor-vacancy complex: $Si_{Ga}$ subsurface and $V_{Ga}$ on the surface.

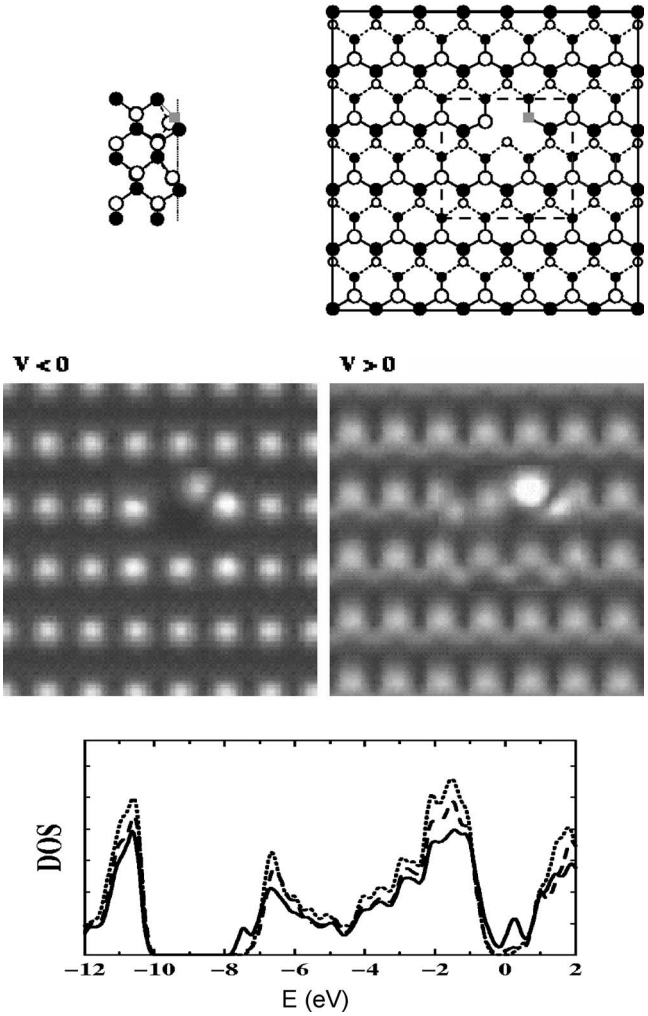


FIG. 18. Donor-vacancy complex: both $Si_{Ga}$ and $V_{As}$ on the surface.

chain; (B) both $Si_{Ga}$ and $Si_{As}$ subsurface, forming again a zig-zag chain; (C) $Si_{Ga}$ atoms on surface and $Si_{As}$ subsurface, forming a row of $Si_{Ga}$-$Si_{As}$ (001)-oriented pairs projected onto the surface; (D) the complementary configuration with $Si_{As}$ atoms on surface and $Si_{Ga}$ subsurface. According to our calculations, configuration B is energetically slightly favoured with respect to the others.

In calculating the STM images, we take into account that the experimental samples of Ref. 16 are overall *n*-doped, and therefore the Fermi energy is close to the bottom of the conduction band. Taking into account that our calculated surface gap is approximately 0.3 eV smaller than the experimental value, the experimental data at $V_b = -1.7$ V and $V_b = 1.3$ V have to be compared with our calculations at $V_b \approx -1.5$ V and $V_b \approx 1.2$ V, respectively. These values are considered in Figs. 12–15. A general feature that we can observe is a very bright signal at negative bias voltages which is attenuated at positive voltages, weakly or strongly depending on the specific case. With lower resolution, the bright signal would appear as a line of 1–1.5 nm wide, i.e., of dimension comparable with those reported in Ref. 3. The charge state has little influence on the XSTM image of this structures (results not shown here), apart from the negative charge state of C and D, where a weakly bright signal remains also at positive voltages.

It is therefore remarkable that the Si donor-Si acceptor bilayer shows in general STM images which well compare with the experimental observations discussed in this work. We stress that self-compensation seems to be the crucial ingredient for such fingerprints in STM images, as it appears also for lower Si doping. Infact, coming to a Si single monolayer uniformly distributed over two adjacent (001) atomic layers, i.e., with one substitutional impurity every two atoms, the overall features found for the full bilayer also show in this case. In particular, the bright/attenuated contrast at negative/positive bias remains a characteristic feature also in configurations with a reduced local concentration of Si dopants, which are more likely to occur in real samples.

We also notice that self-compensated configurations are also energetically favored with respect to others, since they avoid the presence of uncompensated charges.

## IV. CONCLUSIONS

We complete our study considering also other representative kinds of defects, which could also be present in Si-doped

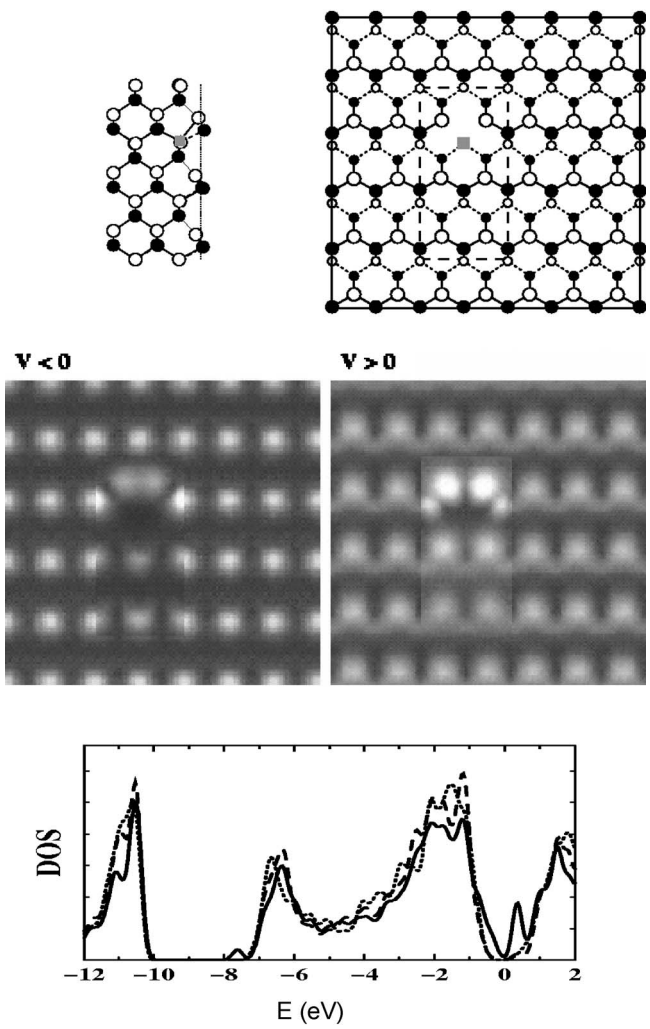


FIG. 19. Donor-vacancy complex: $Si_{Ga}$ subsurface and $V_{As}$ on the surface.

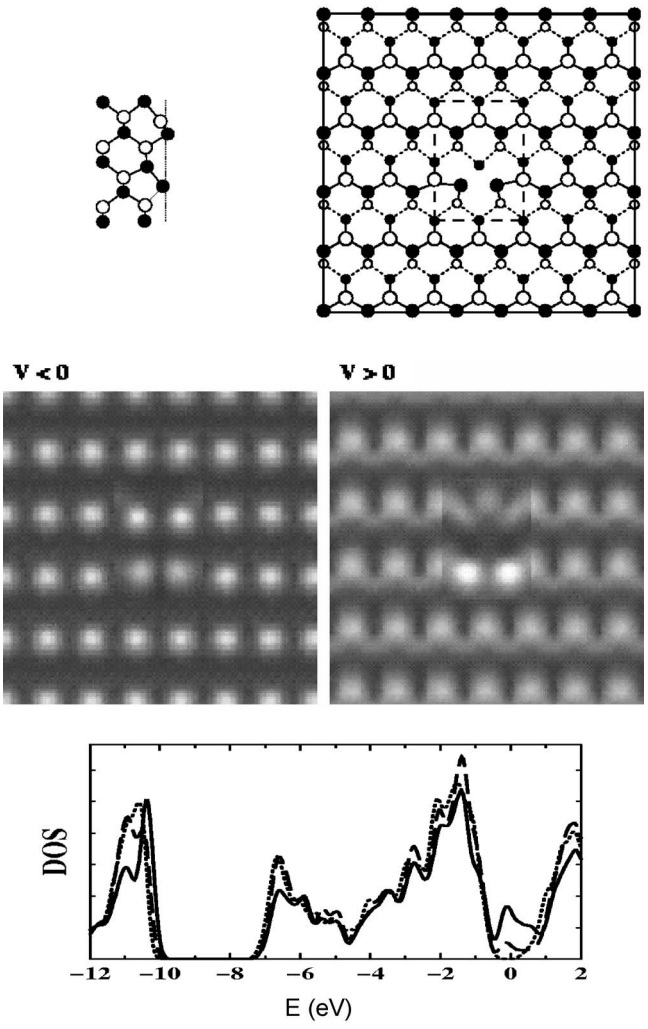


FIG. 20. Isolated $V_{Ga}$ on the surface.

samples: vacancies, antisites, vacancy-impurities pairs. We find (see Appendix) that none of these structures is a good candidate as responsible of the peculiar features of the experimental STM images discussed here.

We can therefore conclude that only for donor-acceptor based configurations where the concentration of Si impurities is the same on cationic and anionic sites, the scenario is consistent with such experimental features. Other configurations can give similar images, but only for a particular bias voltage, and not for negative/positive voltages.

Furthermore, we have studied the dependence of the surface electronic structure on the impurities depth with respect to the exposed surface, and found that subsurface impurities have in general weaker effects than surface impurities.

In spite of the uncertainties due to several factors (tunneling voltage, nature and shape of the tip in case of experiments, specific technical details of the numerical simulations) not fully under control, our findings provide a qualitatively correct picture of the microscopic mechanism responsible for the observed images, thus pointing to the value of first-principles simulations as a tool for the characterization of materials.

## ACKNOWLEDGMENTS

We gratefully acknowledge useful discussions with S. Modesti and A. Franciosi from INFM-TASC National Laboratory in Trieste. This work was supported, in part, by the Italian National Institute for the Physics of Matter (INFM) under Project No. PRA-XSTMS and the "Iniziativa Trasversale di Calcolo Parallelo." One of us (M.P.) also acknowledges support for computational facilities provided by the University of Trieste under the agreement with the Consorzio Interuniversitario CINECA.

## APPENDIX A: COMPLEX DEFECTS INVOLVING $Si_{Ga}$ AND VACANCIES

Taking into account the presence of complex defects opens a wide range of possible configurations, even for the simple donor-vacancy pairs. Many different configurations are possible by varying both the kind of vacancy and the position of the complex defect with respect to the exposed surface. Some complex defects are characterized by an asymmetric shape which easily allows to discriminate them

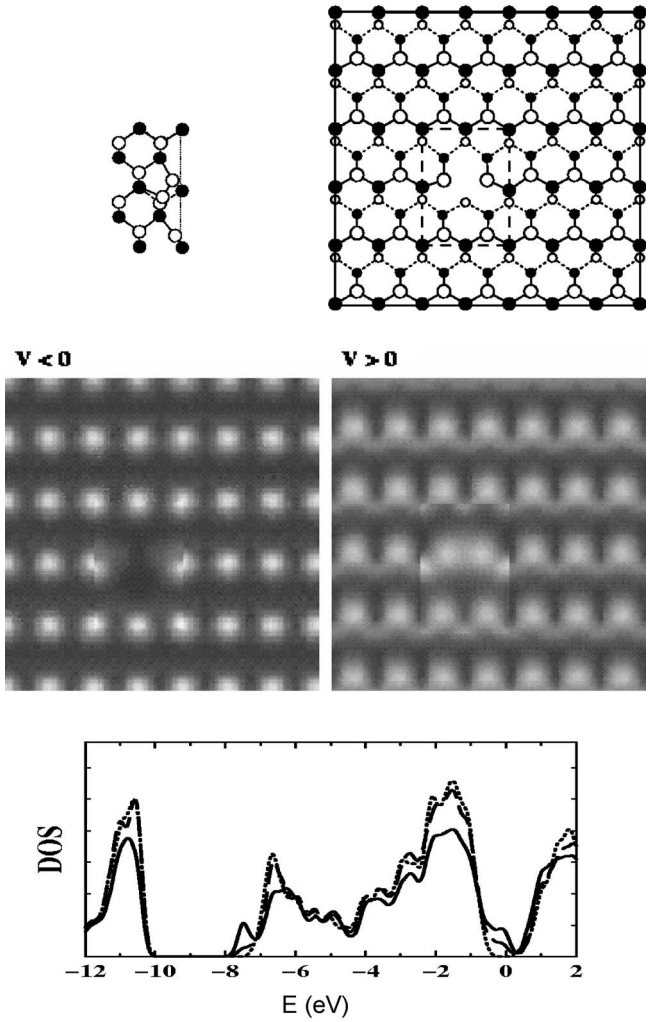


FIG. 21. Isolated $V_{As}$ on the surface.

from single isolated defects (impurities, vacancies, antisites) which show instead regular symmetric features.

#### 1. $Si_{Ga}$-$V_{Ga}$ complex

In Fig. 16 we show the STM images corresponding to a complex defect on surface, namely, a $Si_{Ga}$ close to a vacancy of Ga ($V_{Ga}$), which are next nearest neighbors in the same surface zig-zag bond chain. With respect to the other structures previously discussed, this complex gives rise to asymmetric features in STM images. It corresponds to a rather complex structure in terms of DOS induced in the gap, and this makes the images very sensitive to the applied bias voltage. At positive bias, one empty dangling bond in the Ga surface chains is missing ($V_{Ga}$), whereas others features appear enhanced: they correspond mainly to $Si_{Ga}$ and to its neighboring As which is also close to the vacancy: the result is a bright spot slightly elongated and tilted along the direction of a surface Si-As bond. At negative bias, the complex defect gives rise to a structure composed by a dark region (corresponding to a lack of occupied states for the surface As which is neighbor to $V_{Ga}$) close to a brighter spot (corresponding to an increase of occupied-state of another As

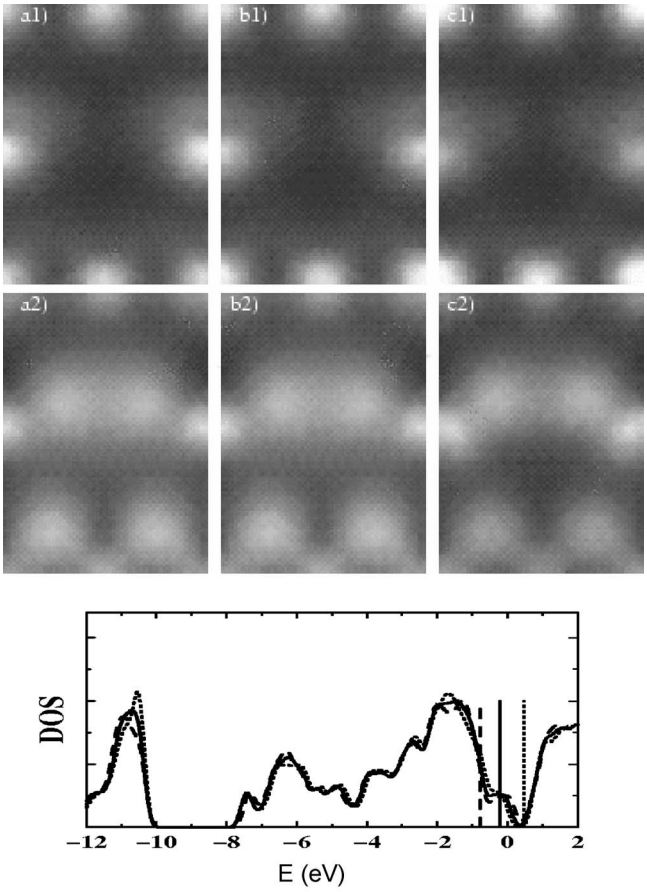


FIG. 22. Isolated $V_{As}$ on the surface with different charge state (−1, 0, and +1 electron for defect). See Fig. 3 for caption.

which is simultaneously neighbor to $V_{Ga}$ and to $Si_{Ga}$).

This complex can have also other geometries which give rise to different STM images. Figure 17 shows for instance the case where the $Si_{Ga}$ is subsurface. In this case, at negative bias there is also a reduction of occupied states with respect to the clean surface, but it is rather delocalized. At positive voltages, a bright elongated feature corresponding to the empty states of the As nearest neighbor to the vacancy is visible parallel to and displaced from the Ga row with the vacancies.

We can conclude that an asymmetric dark/bright structure could be the fingerprint of the complex defect $Si_{Ga}$-$V_{Ga}$ on the exposed surface, with slightly different features depending on the specific position of the Si impurity. Our simulated images compare well with the experimental ones reported in Refs. 29 and 33 and attributed to this kind of defect, in particular for the strong evidence of a lack of empty states due to the surface $V_{Ga}$; other minor features are more difficult to compare.

#### 2. $Si_{Ga}$-$V_{As}$ complex

Another complex defect involving Si donors is that with a vacancy of As. Two possible geometries and the corresponding electronic features are show in Figs. 18 and 19, according whether the Si impurity is on surface or subsurface, whereas $V_{As}$ is always on the surface.

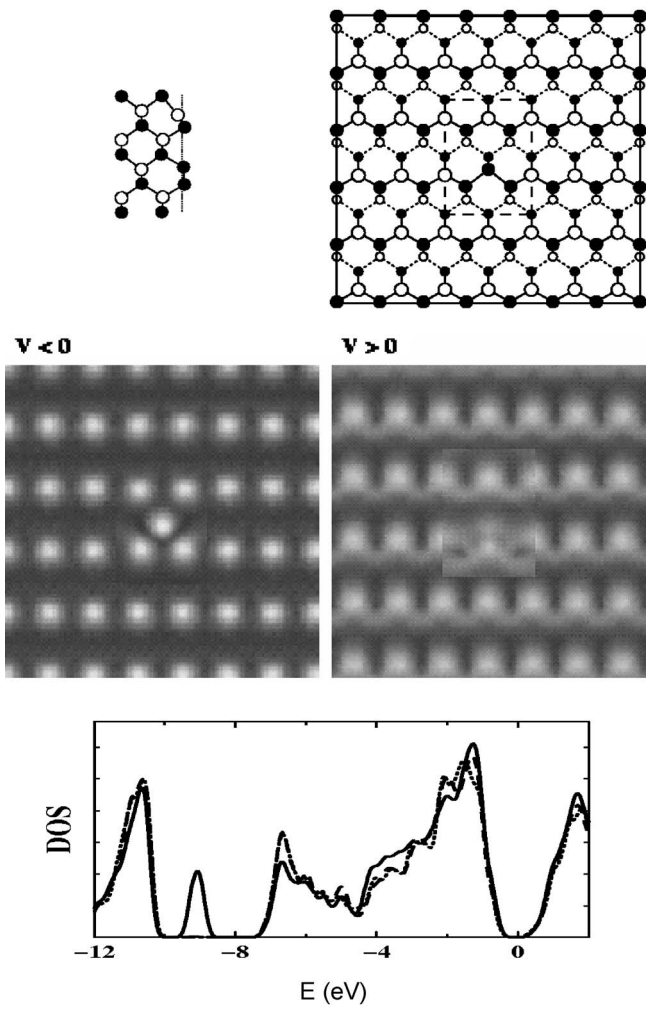


FIG. 23. $As_{Ga}$ antisite on the surface.

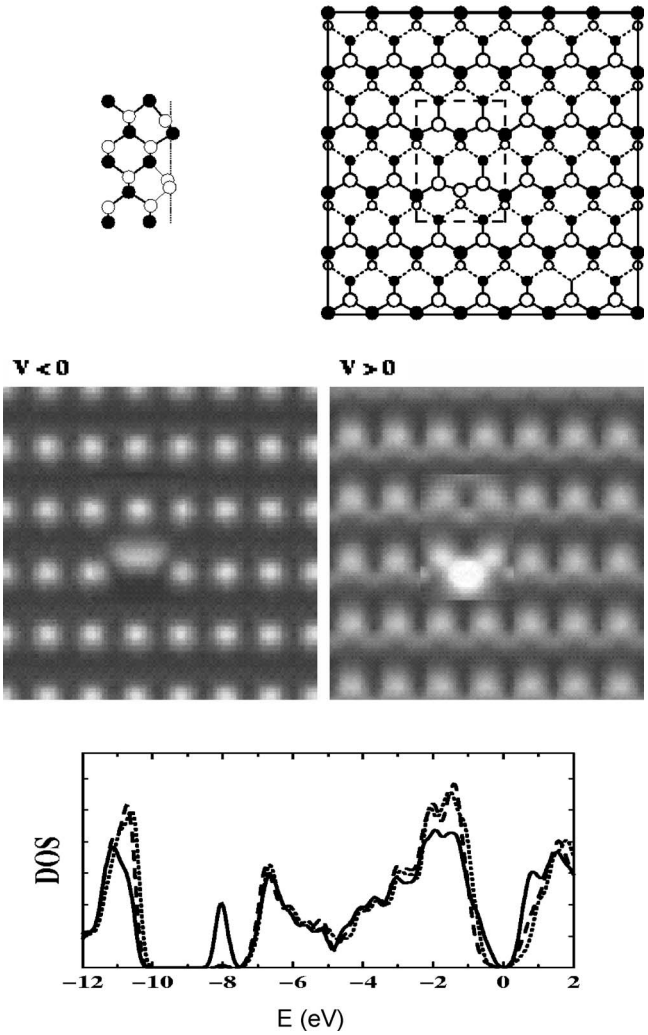


FIG. 24. $Ga_{As}$ antisite on the surface.

The common feature in both cases is the lack of occupied states due to the $V_{As}$ in the surface As images, resulting in a dark structure off-centered with respect to the surface As sites. Then, in Fig. 18 it is evident the surface $Si_{Ga}$, visible with its occupied states at negative voltages with an additional structure with respect to the rows of As, and even more visible as empty states at positive voltages. For this latter feature, because of the presence of a surface $Si_{Ga}$, Fig. 18 resembles Fig. 2, showing the case of the isolated surface $Si_{Ga}$.

Experimental images attributed to this kind of complex defect are shown in Ref. 29 and reported also in Refs. 34 and 35. These images are consistent with our calculated plots for their main features, in particular for the dark structure at negative bias and the well defined, Ga-centered bright spot at positive bias.

In Fig. 19 the dark structure due to the lack of occupied states is also clear, whereas the bright structures of the empty states are much more delocalized with respect to the previous Fig. 18, corresponding to two surface Ga close to the vacancy.

## APPENDIX B: OTHER SIMPLE DEFECTS NOT INCLUDING Si: VACANCIES AND ANTISITES

We complete the investigation of the simplest defects in Si doped GaAs by considering for comparison defects which do not involve doping impurities, but could be intrinsic defects of the host semiconductor or induced by cleavage: these are vacancies and antisites.

### 1. $V_{Ga}$ on the surface

Surface vacancies are accompanied by sizable lattice distortions. In case of $V_{Ga}$ on the surface, the two adjacent As atoms are considerably displaced as it can be seen both from our ball and stick model and also from the imaging of their filled states in the STM plots (negative bias) in Fig. 20.

The $V_{Ga}$ on the surface induces a reduction of empty states in correspondence to the vacancy itself, which corresponds to a darker region in STM images at positive bias.

The Ga vacancy is accompanied by midgap states originating from the two surface As adjacent to the vacancy which give rise—in our simulated images—to a pair of bright spots in particular at rather small (almost $\leqslant 1$ eV)

positive voltages. This feature however is rather controversial: in some experimental images, as for instance reported in Ref. 29, a bright double spot attributed to $V_{Ga}$ appears at −2.4 eV, without being surrounded by darker regions, whereas a dark region extending over the vacancy and adjacent atoms is detected at +1.8 eV. In Ref. 3 dark areas for $V_{Ga}$ are observed at negative bias.

In this case the simulated STM image is very sensitive also to small changes of the bias voltage, for instance, the As pair neighbor to the vacancy is very bright at +1 eV and drastically less bright at ≈2 eV. Incidentally, we note that our image at negative bias is very similar to that shown in Ref. 38 for $V_{Ga}$ on the (110) GaP surface.

The two surface As that would be bond with the missing Ga rebonds to the As subsurface. Their distance is 2.84 Å, which is approximately 19% larger than the surface Ga—As bond length (both atoms on surface). Our conclusion about the formation of As-As bonds (already proposed in Ref. 11) is not based just on a geometric criterion, but on a careful analysis of the bonding pattern through the charge density distribution and the *electron localization function* (ELF).[39] The ELF, a scalar function of the position, measures the conditional probability of finding an electron in the neighborhood of another electron with the same spin. High values of both the charge density and the ELF functions in the same region of space indicate unambiguously the presence of a bond, as it occurs in the present case along the line joining the surface and subsurface As. Conversely, low values of the charge density and high values of the ELF would indicate the presence of a dangling bond.

#### 2. $V_{As}$ on surface

$V_{As}$ on surface has been identified experimentally[40] and also studied by first-principles.[11,12,41] As shown in the ball and stick model in Fig. 21, surface Ga atoms adjacent to the vacancy relax further inward with respect to the clean surface. The surface buckling near the vacancy is 0.92 Å. The distance between surface and subsurface Ga atoms is 2.67 Å, which is 12% larger than the surface Ga-As bond length (both on surface). Similarly to the complementary case of $V_{Ga}$ previously discussed, the strong lattice distortion is accompanied by the formation of a bond between the surface Ga atoms NN to $V_{As}$ and the neighboring Ga atoms in the subsurface layer. This rebonding has also been suggested in Ref. 11.

The charge state affects the induced structural relaxations and the relative position of the electronic bands and the Fermi energy. Both in case of negative and positive charge state, we found that the two surface Ga atoms NN to the vacancy relax inward, in agreement with Ref. 11, while the surface buckling near the vacancy are 1.03 Å and 0.94 Å for the negative and positive charged states, respectively. With the same criterion of comparing electron density distribution and localization function used for the neutral case, also for the charge states we find a rebonding of surface with subsurface Ga in the neighboring of $V_{As}$, the weak bond length being 2.52 Å (in agreement with the value 2.54 Å in Ref. 11) and 2.80 Å long, respectively. Concerning the electronic properties, we notice that the main effect of the charge state is a relative shift of the DOS with respect to the Fermi energy. However, the relative position of the defect state with respect to the gap edges do not change dramatically, and consequently the STM images referred to a Fermi energy in the midgap remain qualitatively the same (Fig. 22). Details on the structural and electronic properties of the charged configurations of As vacancy have been discussed also in Refs. 11 and 40.

It is interesting to note that the STM imaging for this configuration can be consider only as a qualitative indication of the atomic positions. Infact, from the STM images at positive bias in Fig. 22 the two bright spots corresponding to surface Ga appear much closer than others although their actual distance (3.912 Å, 3.9 Å, and 4.00 Å) is close to or even larger than the corresponding one in the clean surface (3.93 Å).

#### 3. $As_{Ga}$ and $Ga_{As}$ antisites

$As_{Ga}$ antisites near the surface have been extensively studied, both theoretically[14,15,42] and experimentally.[43,44] According to whether $As_{Ga}$ is on the surface layer or subsurface, different stable or metastable structures are possible, giving specific image patterns of filled and empty states. Antisites can have very unusual atomic-scale configurations related to large displacements along the {111} directions which may even cause a change in the coordination.[15] We consider here only the configuration of the $As_{Ga}$ antisite located just on the surface; it tends to recover the ideal zinc blende atomic position, thus making the surface buckling almost vanishing, as shown in Fig. 23 (top left panel) and found also in Ref. 42 [Fig. 4(j)]. At variance with subsurface configurations which have been shown to be similar to bulk configurations in terms of electronic effects, $Si_{Ga}$ on the surface does not show localized midgap states; this can be observed from the DOS reported on the bottom panel of Fig. 23. It is visible, instead, a pronounced peak in the ionicity gap. Although the highest occupied state is delocalized,[42] the imaging of filled states only slightly below the valence band top (for bias voltages of −1 eV or similar values) shows a localized signal corresponding to the $As_{Ga}$ atom which appears as an additional interstitial bright spot with respect to the normal As imaging, as it can be seen from the central panel of Fig. 23. A much more delocalized structure appears at positive bias (see Fig. 23). Our results compare well with the observed STM images.[43] attributed to this kind of defect. They differ instead with those of the $As_{Ga}$ subsurface.[44]

The cation antisite ($Ga_{As}$) on surface relaxes inward with respect to the substituted As surface atoms (see Fig. 24). The $Ga_{As}$ moves up along the (001) direction, so that the bonds with its NN Ga on surface and with its NN Ga in the second layer are slightly shorter than the original Ga-As bond.

From the STM images we can see at negative bias voltage a black region corresponding to the antisite position, similar to the anion vacancy, accompanied by a bright region displaced with respect to the As images. We should caution the reader that this feature is sensitive to the applied bias voltage, and strongly attenuates increasing the bias toward more

negative values. At positive bias voltage the fingerprint of the antisite is much more clear, resulting in a brighter spot with respect to the images of the other Ga atoms, and two less bright surface NN Ga atoms. These bright spots remain evident also at higher voltages (not shown here). Also in this case the LDOS shows an additional peak in the ionicity gap.


[1] R. M. Feenstra, Phys. Rev. B **50**, 4561 (1994).
[2] Ph. Ebert, Surf. Sci. Rep. **33**, 121 (1999).
[3] S. Modesti, R. Duca, P. Finetti, G. Ceballos, M. Piccin, S. Rubini, and A. Franciosi, Phys. Rev. Lett. **92**, 086104 (2004).
[4] N. D. Jäger, E. R. Weber, K. Urban, and Ph. Ebert, Phys. Rev. B **67**, 165327 (2003).
[5] N. D. Jäger, Ph. Ebert, K. Urban, R. Krause-Rehberg, and E. R. Weber, Phys. Rev. B **65**, 195318 (2002).
[6] N. D. Jäger, E. R. Weber, and M. Salmeron, J. Vac. Sci. Technol. B **19**, 511 (2001).
[7] G. J. de Raad, D. M. Bruls, P. M. Koenraad, and J. H. Wolter, Phys. Rev. B **66**, 195306 (2002).
[8] G. J. de Raad, D. M. Bruls, P. M. Koenraad, and J. H. Wolter, Phys. Rev. B **64**, 075314 (2001).
[9] P. Sutter, P. Zahl, E. Sutter, and J. E. Bernard, Phys. Rev. Lett. **90**, 166101 (2003).
[10] J. Wang, T. A. Arias, J. D. Joannopoulos, G. W. Turner, and O. L. Alerhand, Phys. Rev. B **47**, 10326 (1993).
[11] S. B. Zhang and A. Zunger, Phys. Rev. Lett. **77**, 119 (1996).
[12] H. Kim and J. R. Chelikowsky, Phys. Rev. Lett. **77**, 1063 (1996); Surf. Sci. **409**, 435 (1998).
[13] John E. Northrup and S. B. Zhang, Phys. Rev. B **47**, R6791 (1993).
[14] R. B. Capaz, K. Cho, and J. D. Joannopoulos, Phys. Rev. Lett. **75**, 1811 (1995).
[15] S. B. Zhang, Phys. Rev. B **60**, 4462 (1999).
[16] X. M. Duan, S. Baroni, S. Modesti, and M. Peressi (unpublished).
[17] S. Baroni, A. Dal Corso, S. de Gironcoli, and P. Giannozzi, http://www.pwscf.org.
[18] J. Tersoff and D. R. Hamann, Phys. Rev. Lett. **50**, 1998 (1983); J. Tersoff and D. R. Hamann, Phys. Rev. B **31**, 805 (1985).
[19] C. J. Chen, Phys. Rev. Lett. **65**, 448 (1990); Phys. Rev. B **42**, 8841 (1990).
[20] M. Chen, P. G. Clark Jr., T. Mueller, C. M. Friend, and E. Kaxiras, Phys. Rev. B **60**, 11783 (1999).
[21] P. Sautet, J. C. Dunphy, and M. Salmeron, Surf. Sci. **364**, 335 (1996).
[22] M. Di Ventra and S. T. Pantelides, Phys. Rev. B **59**, R5320 (1999).
[23] K. Cho and J. D. Joannopoulos, Phys. Rev. Lett. **71**, 1387 (1993).
[24] S. H. Ke, T. Uda, R. Pérez, I. Stich, and K. Terakura, Phys. Rev. B **60**, 11631 (1999).
[25] B. Engels, P. Richard, K. Schroeder, S. Blügel, Ph. Ebert, and K. Urban, Phys. Rev. B **58**, 7799 (1998).
[26] Guo-Xin Qian, Richard M. Martin, and D. J. Chadi, Phys. Rev. B **37**, 1303 (1988).
[27] Ph. Ebert, B. Engels, P. Richard, K. Schroeder, S. Blügel, C. Domke, M. Heinrich, and K. Urban, Phys. Rev. Lett. **77**, 2997 (1996).
[28] B. K. Agrawal, S. Agrawal, and P. Srivastava, Surf. Sci. **408**, 275 (1998).
[29] C. Domke, Ph. Ebert, M. Heinrich, and K. Urban, Phys. Rev. B **54**, 10288 (1996).
[30] C. Domke, Ph. Ebert, and K. Urban, Surf. Sci. **415**, 285 (1998).
[31] Ph. Ebert and K. Urban, Phys. Rev. B **58**, 1401 (1998).
[32] J. F. Zheng, X. Liu, N. Newman, E. R. Weber, D. F. Ogletree, and M. Salmeron, Phys. Rev. Lett. **72**, 1490 (1994).
[33] J. Gebauer, R. Krause-Rehberg, C. Domke, Ph. Ebert, and K. Urban, Phys. Rev. Lett. **78**, 3334 (1997).
[34] C. Domke, Ph. Ebert, and K. Urban, Phys. Rev. B **57**, 4482 (1998).
[35] J. Gebauer, R. Krause-Rehberg, C. Domke, Ph. Ebert, K. Urban, and T. E. M. Staab, Phys. Rev. B **63**, 045203 (2001).
[36] M. Peressi, S. Baroni, R. Resta, and A. Baldereschi, Phys. Rev. B **43**, 7347 (1991).
[37] G. Biasiol, L. Sorba, G. Bratina, R. Nicolini, A. Franciosi, M. Peressi, S. Baroni, R. Resta, and A. Baldereschi, Phys. Rev. Lett. **69**, 1283 (1992).
[38] G. Schwarz, A. Kley, J. Neugebauer, and M. Scheffler, Phys. Rev. B **58**, 1392 (1998).
[39] A. D. Becke and K. E. Edgecombe, J. Chem. Phys. **92**, 5397 (1990).
[40] G. Lengel, R. Wilkins, G. Brown, M. Weimer, J. Gryko, and R. E. Allen, Phys. Rev. Lett. **72**, 836 (1994).
[41] J. Y. Yi, J. S. Ha, S. J. Park, and E. H. Lee, Phys. Rev. B **51**, 11198 (1995).
[42] Yusuke Iguchi, Takeo Fujiwara, Akira Hida, and Koji Maeda, Phys. Rev. B **71**, 125328 (2005).
[43] Ph. Ebert, P. Quadbeck, K. Urban, B. Henninger, K. Horn, G. Schwarz, J. Neugebauer, and M. Scheffler, Appl. Phys. Lett. **79**, 2877 (2001).
[44] R. M. Feenstra, J. M. Woodall, and G. D. Pettit, Phys. Rev. Lett. **71**, 1176 (1993).